NOVEL LIQUID AND BROADBAND CIRCULARLY-POLARIZED ANTENNAS FOR WEARABLE BIOMONITORING APPLICATIONS

A Thesis
Presented to
The Academic Faculty

by

Anya N. Traille

In Partial Fulfillment
of the Requirements for the Degree
MS in the
School of Electrical and Computer Engineering

Georgia Institute of Technology
December 2009

NOVEL LIQUID AND BROADBAND CIRCULARLY-POLARIZED ANTENNAS FOR WEARABLE BIOMONITORING APPLICATIONS

Approved by:

Dr. Manos M. Tentzeris, Advisor
School of ECE
Georgia Institute of Technology

Dr. Joy Laskar
School of ECE
Georgia Institute of Technology

Dr. Gerald DeJean
School of ECE, Adjunct / Microsoft Research
Georgia Institute of Technology

Date Approved: November 2009

ACKNOWLEDGEMENTS

I wish to thank Charlene Reid, temporary Administrative Assistant in the Graduate Thesis Office through Spring 2005, for developing the original version of this style document.

TABLE OF CONTENTS

LIST OF TABLES

LIST OF FIGURES

LIST OF SYMBOLS AND ABBREVIATIONS

RFID	Radio-Frequency Identification
LF	Low Frequencies
HF	High Frequencies
UHF	Ultra-High Frequencies
RF	Radio Frequencies
EEG	Electroencephalogram
ECG	Electrocardiogram
EMG	Electromyogram
FDTD	Finite-Difference Time-Domain
VSWR	Voltage Standing Wave Ratio
CP	Circular Polarization
AR	Axial Ratio
TLM	Transmission Line Method
SBA	Short backfire antenna

SUMMARY

The explosive growth of the biosensors and health-related wearable monitoring devices has accentuated the need for miniaturized, high-efficiency conformal bio-modules that can operate over a wide range of frequencies, while they can be integrated in wearable and lightweight configurations. One of the major issue for the implementation of Wireless Body Area Networks (WBAN) is the very limited range of commonly used metal antennas. Due to the high dielectric constant between the metal antenna material (as well as the metal-based circuitry) and the mostly "ionized-water" human body parts, the near-field gets significantly disturbed, while local reflections due to the dielectric mismatch further shorten the operation range. Even wearable bracelet-like sensing devices have a very low range due to this reason. Thus, there are two major aspects that are going to be addressed in this Thesis: enhanced-range wearable antennas for wireless biosensors and compact "rugged-polarization" wireless sensor readers.

CHAPTER 1

INTRODUCTION TO

BIOMONITORING AND BIOMATERIALS

The explosive growth of the biosensors and health-related wearable monitoring devices has accentuated the need for miniaturized, high-efficiency conformal bio-modules that can operate over a wide range of frequencies, while they can be integrated in wearable and lightweight configurations. One of the major issues for the implementation of Wireless Body Area Networks (WBAN) is the very limited range of commonly used metal antennas. Due to the high dielectric constant between the metal antenna material (as well as the metal-based circuitry) and the mostly "ionized-water" human body parts, the near-field gets significantly disturbed, while local reflections due to the dielectric mismatch further shorten the operation range. Even wearable bracelet-like sensing devices have a very low range due to this reason. Thus, there are two major aspects that are going to be addressed in this Thesis: enhanced-range wearable antennas for wireless biosensors and compact "rugged-polarization" wireless sensor readers. Since the dielectric property and the conductivity of aquatic solutions are a function of the salinity level, liquid antennas can be easily reconfigured for different areas of mounting/observation and will be the focus of the last chapter of the Thesis.

Ida has demonstrated the dependence of the efficiency bandwidth on the permittivity of the dielectric surrounding a metal conductor. This dielectric slows the velocity of the electromagnetic energy in the dielectric and leads to physically smaller than the thin wire counterparts for the same frequency. An antenna with a salt solution radiator was published by Hatch, who coined the term "Ionic Liquid Antenna" in 2000, but only indirectly demonstrated its operability in HF frequencies. Encapsulating the proposed liquid antennas in flexible plastic containers makes them quite easily wearable. In addition, corrosion resistance is another advantage of the ionic-liquid, glass/plastic-

enclosed antennas, while the easy elimination of air gaps permits shape manipulation and an improved electromagnetic coupling between the probe and the probed dielectric. Since the dielectric property and the conductivity of these solutions are a function of the salinity level, these antennas can be easily reconfigured for different areas of mounting/observation.

RFID is an emerging compact wireless technology for the identification of objects, and is considered as an eminent candidate for the realization of a completely ubiquitous "ad-hoc" wireless networks. RFID utilizes electromagnetic waves for transmitting and receiving information stored in a tag or transponder to/from a reader. This technology has several benefits over the conventional ways of identification, such as higher read range, faster data transfer, the ability of RFID tags to be embedded within objects, no requirement of line of sight, and the ability to read a massive amount of tags simultaneously [1.1]. A listing of applications that currently use RFID are: retail supply chain, military supply chain, pharmaceutical tracking and management, access control, sensing and metering application, parcel and document tracking, automatic payment solutions, asset tracking, real time location systems (RTLS), automatic vehicle identification, and livestock or pet tracking.

The demand for flexible RFID tags has recently increased tremendously due to the requirements of automatic identification/tracking/monitoring in the various areas listed above. Compared with the lower frequency tags (LF and HF bands) already suffering from limited read range (1-2 feet), RFID tags in UHF band see the widest use due to their higher read range (over 10 feet) and higher data transfer rate [1.2]. The major challenges that could potentially hinder RFID practical implementation are: 1) Cost; in order for RFID technology to realize a completely ubiquitous network, the cost of the RFID tags have to be extremely inexpensive in order to be realized in mass production amounts 2) Reliability; and that extends to primarily the efficiency of the RFID tag antennas, readers, and the middleware deployed, 3) Regulatory Situation; meaning tags

have to abide to a certain global regulatory set of requirements, such as the bandwidth allocations of the Gen2 Protocols defined by the EPC Global regulatory unit [1.3]. Environmentally-friendly materials, in order to allow for the easy disposal of a massive number (in the billions) of RFID's.

This thesis demonstrates for the first time how the combination of liquid antennas with efficient RFID multiband readers can tackle all four challenges enabling the easy implementation of ubiquitous RFID and wireless biosensing networks.

1.1 Biomonitoring Principles and Challenges

Typical bio-monitoring systems simultaneously measure signals from various angles and locations of the body and these numerous 'views' maximize both the accuracy and consistency of bio-signal data. The electrodes are placed in various positions with respect to the tissue being monitored however in addition to electrode contact noise, the 'patient cables' used to carry the signal to the patient unit introduce additional artifacts to the bio monitoring system that prohibit it from providing 'real-time' data recording. Stray effects such as 'power line interference', due to cable loops, instrumentation noise, muscle movement artifacts and IV drip, corrupt cable transferred data. Filters used to eliminate the interference are the current solution; however, their drawbacks are increased cost, reduction in portability, and operator difficulty. In addition, wires create an unnatural environment for the patients as they limit their mobility, also enduing spurious data.

Table 1.1: Commonly used biomonitoring systems [1.4-1.8]

Signal	Bio-source	Strength	Electrode contact or placement	Reading duration
EEG	Radial electric potentials from neurons	10uV-100uV scalp.10mV-20mV subdural	~25 scalp electrodes	20-40min
MEG	Weak magnetic fields produced by synchronized neuronal currents in brain	A Few femtoteslas	Not available	Not available
GSR	Electrical resistance of skin	KOhms	Not available	Not available
ECG	Electrical activity of heart	0.1-0.5mV	Skin Electrodes: RA, LA, LL, RL, V1, V2, V3, V4, V5, V6	Not available
EMG	Activation signal of muscles (electric potential generated by muscle cells)	<50uV to 30 mV	Needle or surface electrodes	Not available

A portable reliable wireless system designed for in vitro operation would allow for real-time simultaneous communication between transmitters placed on various locations of the body to a stationary or portable patient unit, thus eliminating the cable interference problem.

Still, there are numerous limitations that have to be addressed in order to implement biomonitoring devices in large number. First of all, power line interference is a major issue as loops in patient cables cause stray effects and fields due to the significant values of alternating current. Additional noise is introduced due to electrode contact, muscle contraction, electrosurgical equipment and instrumentation in close distance. Signal artifacts such as baseline drift due to physiological and instrument noise [1.9], muscle movement.

Figure 1.1. ECG [1.10] (top left), EEG [1.11] (top right) and EMG [1.12, 1.13] (bottom left, bottom right).

One example can be found in Electro-Engephalograph (EEG) monitoring where Meninges, cerebrospinal fluid and skull introduce excessive attenuation and frequency dispersion [1.4]. Other artifacts are patient induced such as eye blinks and movements, as well as glossokinetic and body/neck motion effects that introduce further artifacts. Other noise/interference sources include EKG-cardiac and EMG-muscle monitoring equipment and excitation waves, electrode pops (spikes originating from momentary changes in impedance values of given electrodes), poor electrode grounding and IV drips. As it is clear, human body and especially the scull, are very challenging environments for wireless and RF monitoring requiring a fundamentally different new paradigm than the conventional metal-based antennas. In this thesis, the foundation of a new generation of bioantennas based on liquid solutions will be introduced for the first time.

1.2 History of Liquid Antenna Systems

High dielectric constant antennas date back to the 1930s where it was shown that conducting liquids and biological fluids could operate as antennas at microwave frequencies. According to reports from The Radio Amateur community, stimulating a column of salt water could produce a usable antenna. It was found that for salt water columns with salinity in excess of 70 ppt, that at HF frequencies under 30 MHz, the resonant frequency was inversely proportional to salt solution column height. Bandwidths increased from 20-25% up to 50% with a radiation efficiency of 50-70%.

Fayad and Record presented reconfigurable liquid antennas at 1-2.5 GHz. They consisted of PVC (polyvinyl chloride) resonator columns filled with liquid, sealed with silicone rubber, mounted on a ground plane and fed with a gold plated steel electrode. It was determined that the operating frequency was dependent on the height of the column however the lossy nature of water at high frequencies indicated the need to explore other

liquid dielectrics [1.14].

Kosta and Kosta used mercury to fabricate a circular liquid microstrip antenna at 8.362 GHz using a pressured glass cavity surrounded by duroid. It was found that the ability to accurately characterize conductive liquids would be needed in order to completely achieve the design concept [1.15].

O'Keefe and Kingsley 50MHz DRA out of water, exploring the reconfigurability by using a pump to adjust the water level. They stressed the challenge of designing and tuning a feeding probe at a wide frequency range. They brought up the challenge of deploying low viscosity liquids suggesting the use of a support matrix, or gels [1.16].

1.3 Properties of Bio-materials

The simplest phantoms assume a homogeneous material consisting of only muscle tissue whereas more complex layered models will include skin, fat and bone. These tissue properties are listed in the tables [1.2-1.7], attached below, using values from [1.17] and measurements performed in the presented work. Additional selected tissues are shown to give a clear idea of extreme value variations found in certain organs. The corresponding plots [Figures 1.4-1.5] give a more detailed representation of the distributions. The dielectric properties of tissue vary depending on the water content [1.18-1.20], as well as molecular structure of the bio material. When comparing all tissues in the body, the largest variation from tissue-to-tissue can be seen at very low frequencies. There are certain tissues (such as the brain), which uniquely exhibit a dip in the loss tangent at low frequencies (from 12Hz to 14Hz).

Table 1.2

Tissue properties at 10 Hz [1.17]			
Tissue	**Conductivity**	**Relative Permittivity**	**Loss Tangent**
*Brain (grey)	0.027512	40699000	1.2151
*Spleen	0.039596	43303000	1.6437
*Cerebellum	0.047512	40700000	2.0984
*Muscle	0.20197	25700000	14.126
*Bone (Cancellous)	0.075563	10020000	13.555
*Fat	0.012207	7973500	2.7519
*Bone (Cortical)	0.020028	55153	652.75
*Skin (Dry)	0.0002	1136	316.47
*GallBladder Bile	1.4	120	20971000
*Body Fluid	1.5	99	27236000
*Virteous Humor	1.5	99	27236000
*CerebroSpinal Fluid	2	109	32983000

At low microwave frequencies the properties of different tissues start to converge; however, it should be noted that low water content tissues such as fat and bone still have significantly lower permittivities than skin and muscle which enclose them. This inhomogenuity presents a need to utilize layered models (Figure 1.2) in practical system simulations in order to take in account the effect of skin absorption and magnetic field gradients within the layers at these frequencies [1.17, 1.21-1.24].

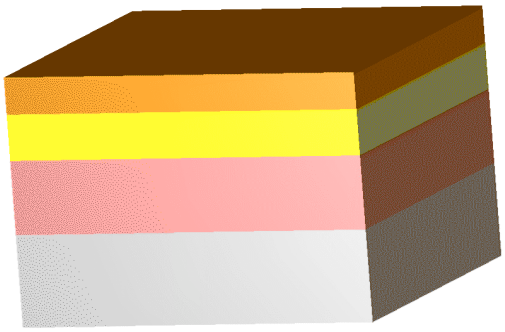

Figure 1.2. Layered Tissue Model *(Starting from top: Skin, Fat, Muscle, Bone)*.

Table 1.3

Tissue Properties at 300MHz **Online Data* [1.17]			
Tissue	**Conductivity**	**Relative Permittivity**	**Loss Tangent**
*Brain (grey)	0.6924	60.022	0.6912
*Spleen	0.96906	66.491	0.87327
*Cerebellum	0.97321	59.719	0.97645
*Muscle	0.77052	58.201	0.79325
*Bone (Cancellous)	0.21556	23.163	0.55761
*Fat	0.039569	5.634	0.42082
*Bone (Cortical)	0.082662	13.439	0.36855
*Skin (Dry)	0.64141	49.821	0.7714
*GallBladder Bile	1.6696	74.886	1.3359
*Body Fluid	1.3161	65.65	1.2012
*Virteous Humor	1.5177	69.017	1.3176

*CerebroSpinal Fluid	2.2245	72.734	1.8325

Table 1.4

Tissue Properties at 400MHz **Online Data* [1.17], ***Measurements Taken*			
Tissue	**Conductivity**	**Relative Permittivity**	**Loss Tangent**
*Brain (grey)	0.73748	57.435	0.57702
*Spleen	1.0259	63.224	0.72919
*Cerebellum	1.0304	55.996	0.82689
*Muscle	0.79631	57.129	0.62639
*Bone (Cancellous)	0.23459	22.443	0.46974
*Fat	0.041119	5.5798	0.33116
*Bone (Cortical)	0.091336	13.147	0.3122
*Skin (Dry)	0.68806	46.787	0.66089
*Gall Bladder Bile	1.6956	72.784	1.0469
*Body Fluid	1.5293	69	0.99599
*CerebroSpinal Fluid	2.2512	70.998	1.4249
**FIJI Water	0.0652	78.4259	0.0374
**Alcohol 50% Isopropyl	0.1078	46.7205	0.1039
**Alcohol 70% Isopropyl	0.1098	36.2322	0.1364
**Alcohol 91%	0.1352	19.2777	0.3156

Isopropyl			
**Listerine	0.1006	65.5922	0.0690
**Bengay	0.1854	25.9582	0.3213
**Ammonia	0.2611	78.1631	0.1503
**Alcohol 70% Ethyl	0.1099	36.6566	0.1349

Table 1.5

Tissue Properties at 910MHz **Online Data* [1.17], ***Measurements Taken*			
Tissue	**Conductivity**	**Relative Permittivity**	**Loss Tangent**
*Brain (grey)	0.94653	52.678	0.35493
*Spleen	1.2776	57.117	0.44184
*Cerebellum	1.2673	49.381	0.50695
*Muscle	0.94637	55.009	0.33984
*Bone (Cancellous)	0.34235	20.766	0.32565
*Fat	0.051282	5.4604	0.18551
*Bone (Cortical)	0.14452	12.444	0.2294
*Skin (Dry)	0.87004	41.354	0.41559
*Gall Bladder Bile	1.8419	70.169	0.51851
*Body Fluid	1.6391	68.889	4.5993
*Virteous Humor	1.6391	68.889	4.5993
*CerebroSpinal Fluid	2.1467	68.617	0.6957
**FIJI Water	0.2126	79.3687	0.0530

**Alcohol 50% Isopropyl	0.4694	44.8034	0.2072
**Alcohol 70% Isopropyl	0.4973	32.9260	0.2988
**Alcohol 91% Isopropyl	0.4185	13.5562	0.6107
**Listerine	0.3960	66.0421	0.1186
**Bengay	0.2979	25.3760	0.2322
**Ammonia	0.4317	77.9821	0.1095
**Alcohol 70% Ethyl	0.5027	34.9544	0.2845

At all microwave frequencies, substrate modes and surface waves (Figure 1.3) create unpredictable effects in the near-field, most of which disrupt the radiation performance making implantable wireless devices unreliable due to the matching limitations.

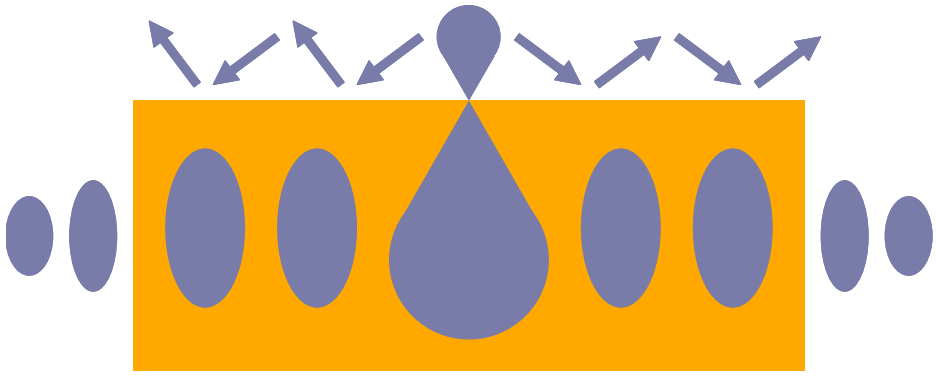

Figure 1.3. Substrate and surface modes in human tissues.

Modifying the radiator design alone cannot compensate for the near-field effects,

however utilizing high permittivity liquid materials will give the benefit of altering matching characteristics to improve performance.

Table 1.6

Tissue Properties at 1.7 GHz **Online Data* [1.17], ***Measurements Taken*			
Tissue	**Conductivity**	**Relative Permittivity**	**Loss Tangent**
*Brain (grey)	1.3341	50.287	0.28053
*Spleen	1.7165	54.101	0.33548
*Cerebellum	1.6541	46.357	0.37729
*Muscle	1.2878	53.683	0.25365
*Bone (Cancellous)	0.55736	19.476	0.30259
*Fat	0.074807	5.3605	0.14756
*Bone (Cortical)	0.25846	11.846	0.2307
*Skin (Dry)	1.146	39.042	0.31037
*Gall Bladder Bile	2.2356	69.164	0.34178
*Body Fluid	1.9762	59.552	0.35089
*Virteous Humor	1.9756	68.62	0.30443
*CerebroSpinal Fluid	2.8531	67.345	0.44797
**FIJI Water	0.7216	78.9011	0.0968
**Alcohol 50% **Isopropyl	1.3615	39.9519	0.3608
**Alcohol 70% Isopropyl	1.2408	27.3025	0.4812

**Alcohol 91% Isopropyl	0.6773	9.2909	0.7718
**Listerine	1.3053	63.4346	0.2179
**Bengay	0.5314	24.3678	0.2309
**Ammonia	0.9547	77.3344	0.1296
**Alcohol 70% Ethyl	1.3140	29.1102	0.4780

Below are the high frequency characteristics of the same tissues for comparison. Cerebro Spinal fluid has the lowest variation in dielectric properties across a wide frequency range. At the highest recorded frequency, Gall Bladder-Bile in particular has the highest conductivity than any other tissue.

Table 1.7

Tissue Properties at 100 GHz **Online Data* [1.17]			
Tissue	**Conductivity**	**Relative Permittivity**	**Loss Tangent**
*Brain (grey)	53.246	7.7561	1.234
*Spleen	57.3512	8.0335	1.2833
*Cerebellum	48.194	7.3768	0.00033732
*Muscle	62.499	8.6307	1.3017
*Bone (Cancellous)	16.041	4.102	0.70291
*Fat	3.5624	2.8891	0.22165
*Bone (Cortical)	8.6554	3.2975	0.47182
*Skin (Dry)	39.433	5.5987	1.266

*Gall Bladder Bile	78.118	8.2107	1.7102
*Body Fluid	77.388	7.0012	1.9869
*Virteous Humor	77.388	7.0012	1.9869
*CerebroSpinal Fluid	76.558	9.2945	1.4806

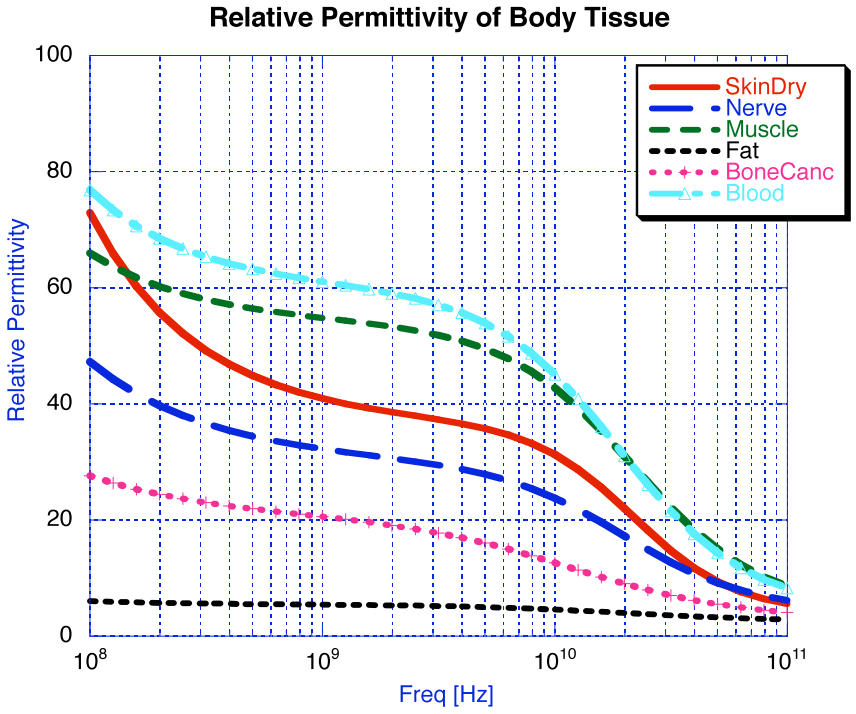

Figure1.4. Relative permittivity of body tissues vs. frequency [1.17].

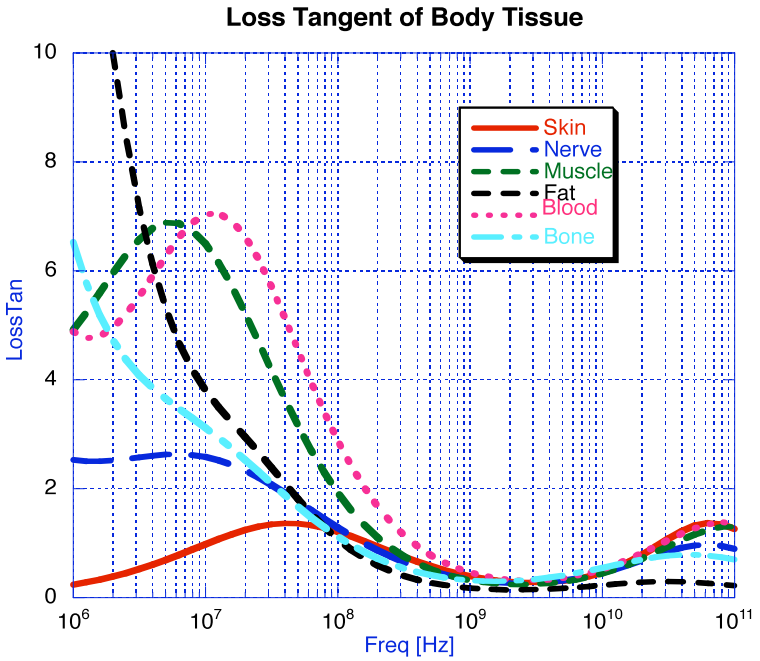

Figure 1.5. Loss Tangent of body tissues vs. frequency [1.17].

1.4 Characterization of Liquid and Gel Materials

To obtain the electrical properties of liquid solutions, material characterization was performed using the Agilent 85870 Dielectric probe kit. This kit was ideally convenient to perform complex permittivity measurements of liquids and semi-solids from 400MHz to 20GHz in a temperature range of -40°C to 200°C and with $\varepsilon_r < 100$ using the Open-ended Coaxial Probe technique [1.25].

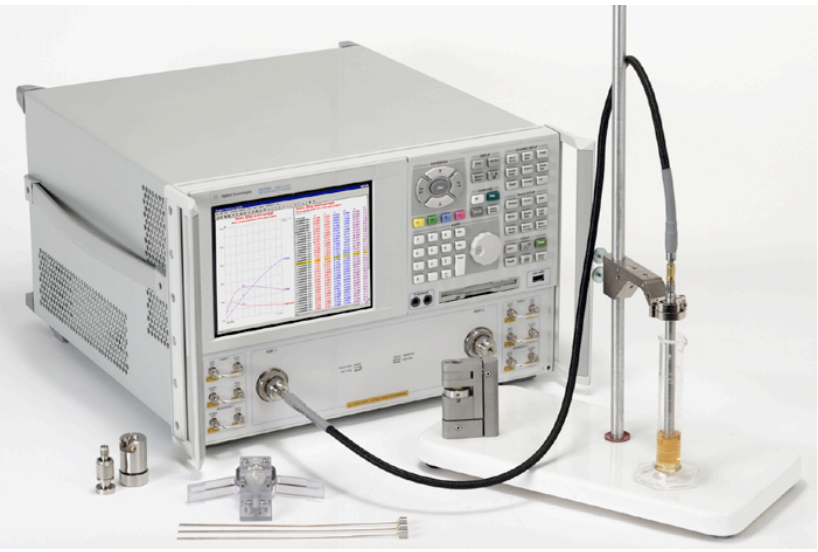

Figure 1.6. Liquid and gel characterization setup.

The measurement setup consisted of a Performance Probe connected to the Vector Network Analyzer through a flexible cable. Cable movement is a significant source of measurement error [1.26] so special care was taken to sturdily mount the probe and restrain the cable. The calibration standard was set to (air/short/water) with the water temperature specified and calibration was performed under the specified frequency sweep by first leaving the probe open in air, then connecting the probe to the shorting block, and finally immersing the probe in distilled water.

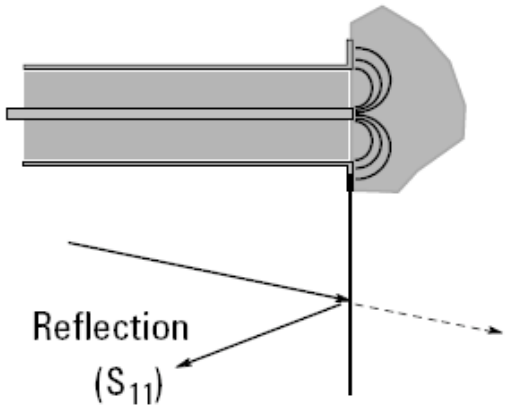

Figure 1.7. Probe placement inside liquid.

To ensure accuracy for liquid measurements, the probe needed to be immersed at least 5mm deep in the liquid, with at least 1mm of solution underneath so that the liquid appears semi-finite in thickness. Air gaps between the probe and solution are a primary source of error as they disrupt the normal E-field components at the end of the probe [1.27].

After calibrating, we tested FIJI Water, Alcohol 50% Isopropyl, Alcohol 70% Ethyl, Alcohol 91% Isopropyl, Listerine, Bengay, Ammonia, Phyto, Pellegrino (to see the effect of moving air bubbles). Tables 1.4-1.6 and Figures 1.8-1.10 show results of the measurements.

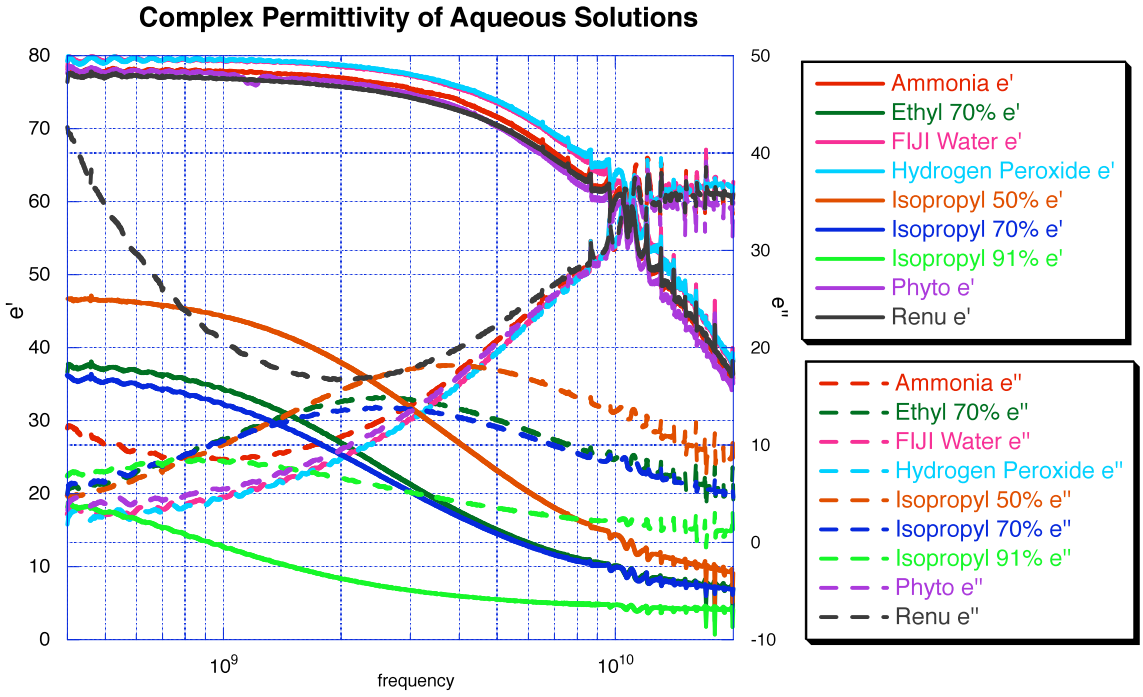

Figure1.8. Measured Complex permittivity vs. frequency for aqueous solutions.

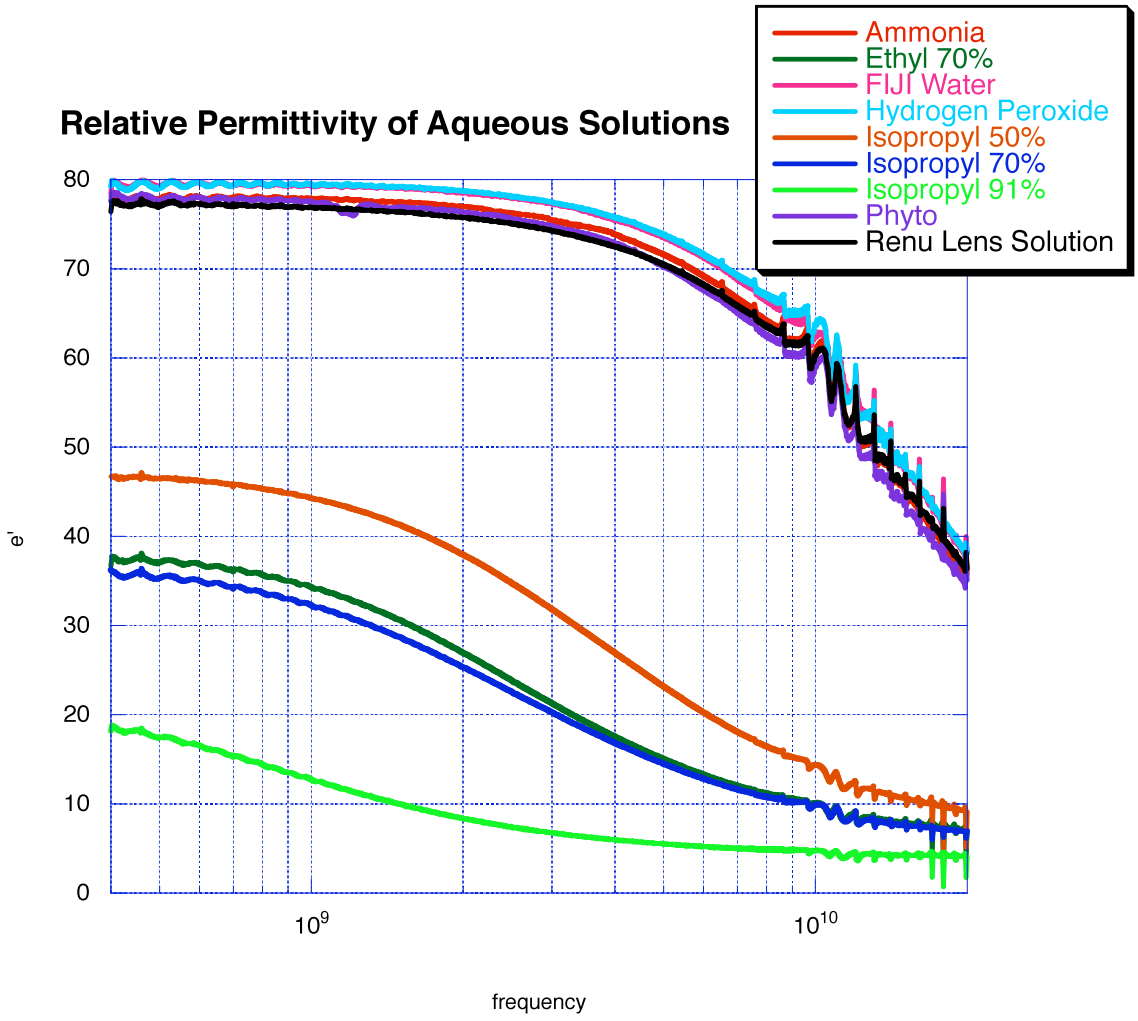

Figure1.9. Measured Relative permittivity vs. frequency for aqueous solutions.

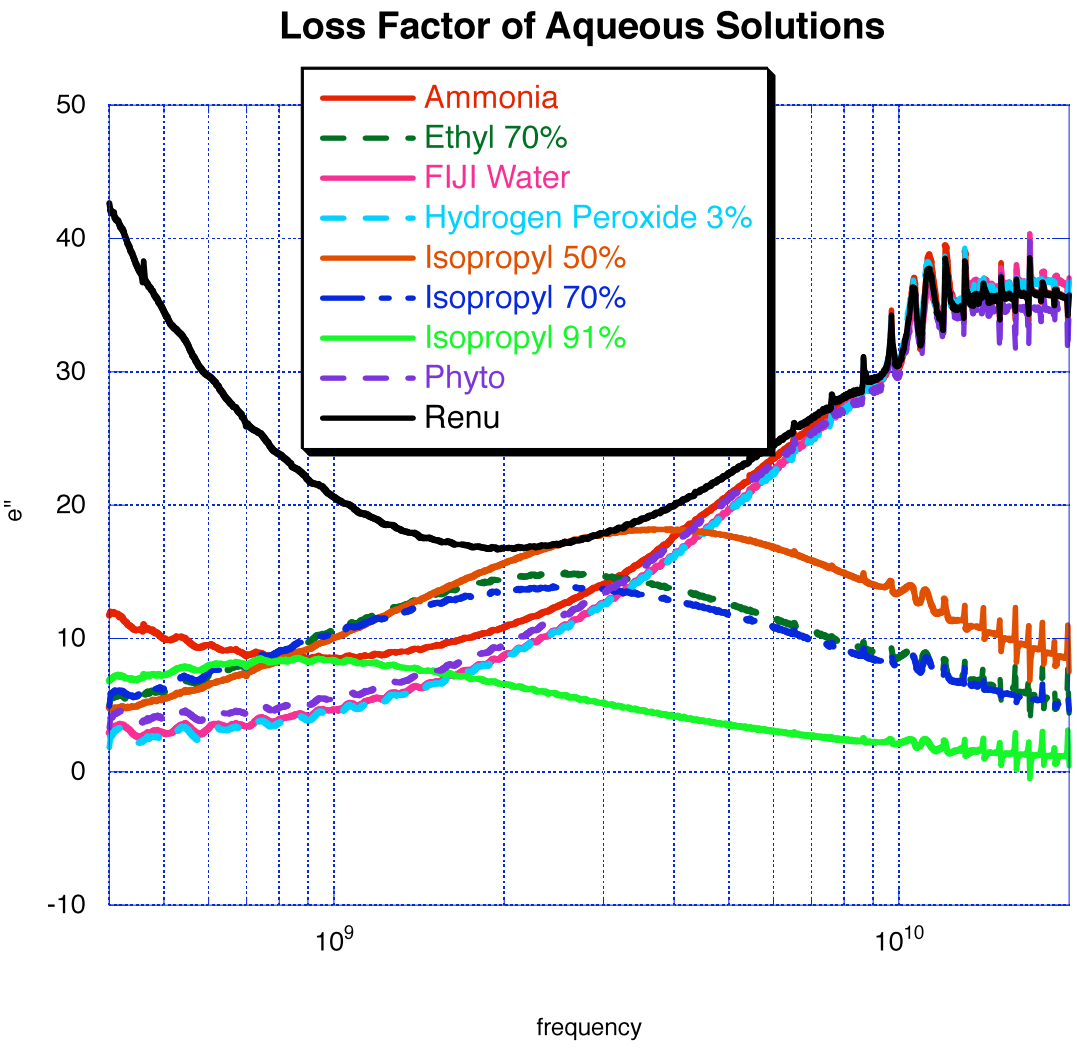

Figure 1.10. Measured Loss Factor vs. frequency for aqueous solutions.

The gel "Phyto" was chosen as the one of the ideal solutions for the liquid antenna design due to it's low loss properties, as well as stability over time, and under movement due to it's gel-like consistency, a concern mentioned in [1.16]. The key feature is that it is non-drying (non-alcoholic), non-greasy, non-coating and non-oily. When kept in a proper sealed container it maintains a gel like consistency. When rubbed onto a surface and left in air to dry it leave a smooth film (think or thin depending on the amount used). Below is the full list of ingredients. Its properties when in thin film form are yet to be examined. The ingredients are listed below:

Althaea Officinalis Root Extract (Mucilage Vegetal), Chamomilla Recutita (Matricaria) Flower Extract (Matricaise), Salvia Officinalis (Sage) Leaf Extract (Sauge), Allium Sativum (Garlic) Bulb Extract, Cochlearia Armoracia (Horseradish) Root Extract (Raifort), Ferula Assa Foetida Root Extract (Ferula), Propylene Glycol, Caprylyl Glycol, Methylisothiazolinone [1.28].

The calibration, measurement, sensitivity calculations and data plots were displayed in the Agilent 85070E Dielectric probe software, then exported, post processed and re-imported into the simulator into various radiator designs. Designs tested or currently under test are the meander, spiral, loop, and hemispherical DRA all in free space and within close vicinity of a human torso or body and some results will be presented in Chapter 4. The human CAD models used (Figure 1.11) were either constructed from scratch or imported from 3DCadbrwser.com, where in the case of pre-built models, geometrical simplification was necessary to reduce simulation time.

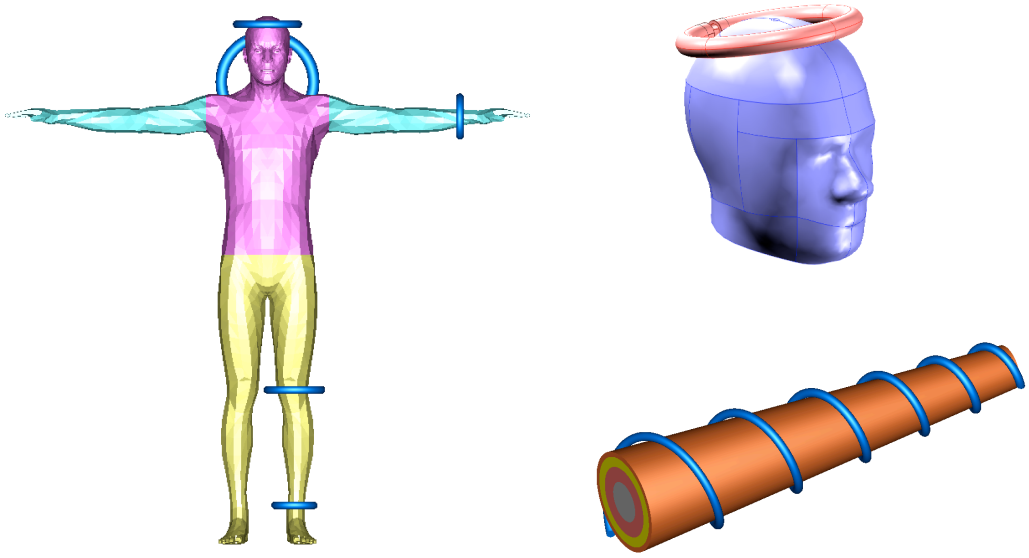

Figure 1.11. CAD models for human body/tissues: Loop antennas positioned on detailed full body model (left), Loop mounted on detailed head (top right), Helix mounted onto simplified Arm with layered tissue added (bottom right).

CHAPTER 2

BROADBAND CIRCULARLY-POLARIZED ANTENNAS FOR WIRELESS BIOMONITORING AND RFID READER SYSTEMS

Modern RFID devices are following the same pattern as the rest wireless/RF devices and components: smaller, faster, cheaper, better, with the additional constraints of low-cost and conformality. In order to meet these requirements a variety of technologies are being integrated into RFID circuits and systems. Advances in paper-based materials and inkjet printing are allowing for thg tighest technology integration today [2.1]. This integration of antennas, matching networks, IC's, batteries and sensors introduces several design challenges. Antennas are one of the most critical RFID components, especially for RFID readers that require universal operation and circular polarization in order to enable operation in different environments and standards (US, Europe, Asia) [2].

Most modern commercial electromagnetic simulators usually employ approximations in order to provide timely results. This leads to inaccuracies, of course, when characterizing structures and phenomena that the simulators are not designed to model, such as components with high aspect ratios and complex features. Full-wave techniques, such as finite-difference time-domain (FDTD) and TLM have higher accuracy, allow for multi-frequency simulation, enable the accurate modeling of the transient effect, however they require "smart" discretization and excitation. This chapter presents the design and modeling of a circular-polarized antenna for universal UHF RFID readers using full-wave time-domain techniques.

2.1 RFID Readers Specs

To satisfy the requirements for the various RFID frequency bandwidth allocations across Europe, USA and ASIA, a global UHF RFID reader must have an antenna that can operate with a least a 9.6% bandwidth from 866 MHz to 954 MHz [2.2]. In addition, this reader has to be "flexible" enabling its functionality in different environments that potentially de-polarize linearly polarized waves (water, food, wood, plants, liquids) [2.3, 2.4]. Finally, numerous RFID readers have to be portable (or quasi-portable), limiting their size to only 12in x 12in.

Existing commercial universal reader antennas are listed in Table 2.1. This data provides a design specification table to represent the effort presented in this paper [2.5, 2.6]. A gain greater than 8 dBi is required for a read range of at least 10m (30-40 ft), while maintaining an axial ratio of less than 2dB is required to guarantee low cross-polarization. In addition, a VSWR less than 2:1 throughout the entire frequency range is also necessary to provide adequate matching with the reader system, and to satisfy power efficiency requirements. It has to be noted that the maximum regulated output power is currently 4 Watts globally.

In addition to the above features, future RFID reader antennas are anticipated to demonstrate the following improvements:

- Mechanical stability to provide portability and resistance against harsh environments [2.4].
- Smaller size, a feature that could challenge the high bandwidth specs [2.4].
- A VSWR decreased down to 1.5:1 (return loss < -14 dB) for even higher power efficiency and range.

Table 2.1: The specs from 2 Cushcraft and 1 Poynting reader antennas (the best currently):

Model	**S8056RC**	**S8658WPC**	**Poynting-A0025**
Frequency	865-965 MHz	865-965 MHz	865-965 MHz
Gain	6 dBi	8 dBi	6.5 dBi
3dB beamwidth	80^o x 80^o	65^o x 65^o	N/A
Polarization	Circular (no axial ratio given)	Circular (no axial ratio given)	Circular (AR<1dB)
VSWR	1.7:1	1.5:1	1.3:1
Dimensions (cm)	21 x 21 x 2.8	25 x 25 x 3.8	24.5 x 23.5 x 4

2.2 RFID Reader Antenna Modeling and Design

About seven years ago, it was found that a dual-rhombic loop can also serve as a broadband CP antenna [2.7]. A bandwidth of 20% for AR<2 dB was obtained for the dual-rhombic loop antenna. The bandwidth of the dual-rhombic loop can be further improved by adding a pair of parasitic rhombic loops inside the original loop [2.8, 2.9]. The impedance matching of the broadband CP antenna is achieved by incorporating a broadband balun into the feeding structure. The gain of the dual-rhombic loop antenna is enhanced by employing it as the excitation element of a short backfire antenna (SBA).

The configuration of a CP dual-rhombic loop antenna is shown in Figure 2.1. The square (W_1 *x* W_1) dual-rhombic loop is printed on a thin square (*Ls x Ls*) dielectric substrate (0.254mm) with a low dielectric constant (RT/Duroid with ε_r=2.2). To radiate a CP wave, a pair of small gaps is introduced on the dual-rhombic loop. A pair of square

(W_2 x W_2) parasitic rhombic loops (also with a small gap) is added inside the dual-rhombic loop for bandwidth enhancement.

An important feature of this loop antenna is that the sense of circular polarization may be adjusted by changing the positions of the small gaps on the loops using RF switches such as microelectromechanical systems or p-i-n diodes. The CP rhombic loop is driven at its center by a broadband balun, which was also fabricated on the same type of RT/duroid 5880 substrate. This kind of broadband balun has been widely used to excite a dipole antenna. The broadband balun can excite the balanced mode by making use of the coupling between the microstrip line printed on one side of the substrate to the slot which is etched on the other side (it also serves as the ground plane for the microstrip line) of the substrate. A good impedance matching can be achieved by adjusting the length (l_s) of the slot, the height (h_m) and the length (l_m) of the microstrip line. The printed CP dual-rhombic loop is backed by a square (L_g xL_g) copper plate (i.e., a ground plane) at a height h for unidirectional radiation and fed through an SMA connector.

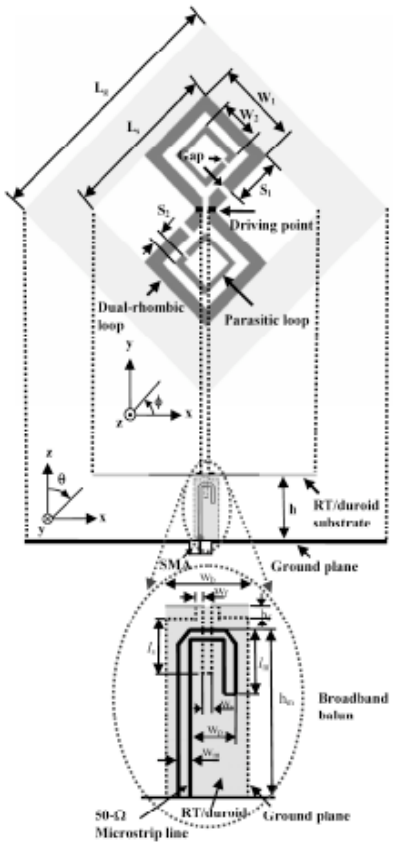

Figure 2.1. Dual-rhombic loop CP antenna.

For simplicity of experimental verification of our simulation results, we designed the above antenna in the frequency range 4-8 GHz. The plan is to scale down this design to 865-965 MHz possibly including the upper DVB band for cellular phone data communication. The modeling and simulation were performed using initially NEC1.1 and then with the full-wave TLM technique (Microstripes 6.5 CAD tool) and the results are shown below.

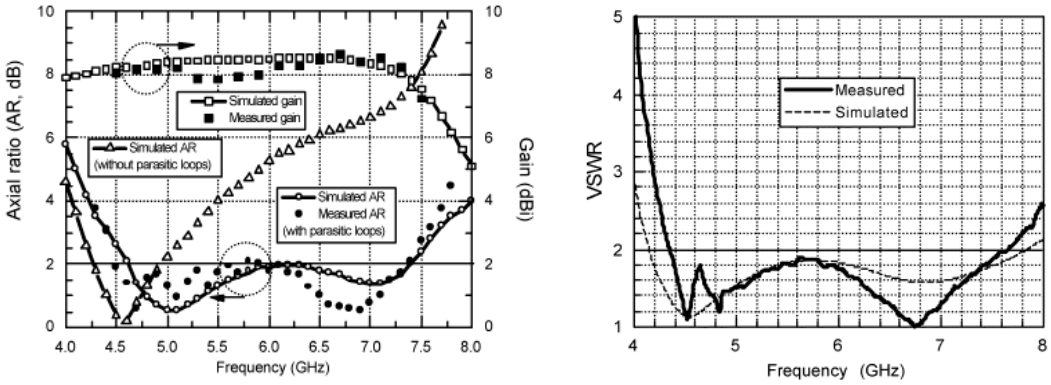

Figure 2.2. ((a)-left) AR, ((b)-right) VSWR of the dual-rhombic antenna.

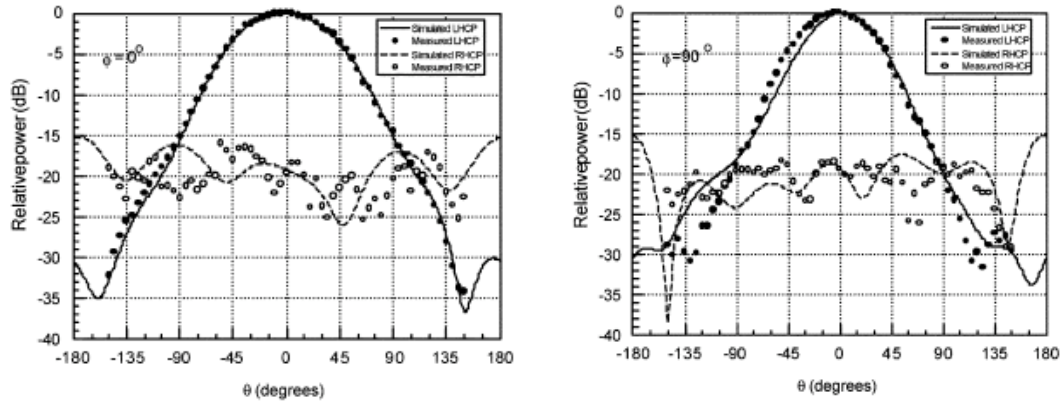

Figure 2.3. Radiation patterns at 6GHz for two principal planes (LHCP: Left-hand-circular-polarization, RHCP: Right-hand-circular-polarization).

It is found (Figure 2.2(a)) that the bandwidth for AR<2dB of the dual-rhombic loop antenna with parasitic loops is about 46%. For comparison, the simulated AR for the dual-rhombic loop antenna without the parasitic loops is also plotted in this figure, which shows a 2-dB AR bandwidth of only 15%. Obviously, the parasitic loops play an important role for the bandwidth enhancement. The reason for this effect is that the dual-rhombic loop can only create one minimum AR point while the parasitic loops can

produce an additional minimum AR point. An appropriate combination of the two minimum AR points leads to a significant enhancement for the CP bandwidth. The gain of the antenna maintains a value around 8 dBi over the 2-dB AR bandwidth. The simulated and measured results for the voltage standing-wave ratio (VSWR) are presented in Figure 2.2(b). The bandwidth for it about 50%, entirely covering the bandwidth. The radiation patterns (Figures 2.3) at 6 GHz at $\phi=0^{o}$ and 90^{o} verify the effective performance of this antenna.

As a conclusion, a very broadband circular-polarization antenna has been modeled and optimized using full-wave numerical techniques for very challenging universal UHF RFID Reader configurations. The design has been verified experimentally for 4-8 GHz, and can be easily scaled down to 865-965 MHz, while offering the opportunity of easily adding services provided by the upper DVB cellular phone band. This is the first time such a system-level design and optimization has been performed using full-wave techniques, that addresses *the issues of radiation pattern, axial ratio and S11 bandwidth, beamwidth and matching, while paying special attention to unique integration design challenges such as the highly capacitively value of RFID IC's and the very stringent size constraints.*

CHAPTER 3

A CAVITY-BACKED BROADBAND CIRCULARLY-POLARIZED SLOT/STRIP LOOP ANTENNA WITH SIMPLE FEEDING

Cavity-backed slot antennas have two major advantages over cavity-backed wire antennas, such as dipole, helix, and spiral antennas [3.1]. First, a slot antenna can be flush mounted on a metal surface; therefore, it is suitable for applications in mobile communications (such as IEEE 802.20 for mobile broadband wireless access) and radar systems of high-speed vehicles or aircraft [3.2]. Second, slot antennas can be easily fed by a microstrip line that is fabricated on the same substrate with the slot and is placed between the cavity and the substrate, thus avoiding the undesirable radiation from the feeding network. This is particularly important for applications in antenna arrays. Many types of slot configurations have been developed for producing circularly polarized (CP) radiation, such as annual slot [3.3], dual-spiral slot [3.4], rectangular slot [3.5], and cloverleaf slot [3.6]. However, these slot antennas have a narrow axial ratio (AR) bandwidth (usually < 5% for AR<3dB). Archimedean spirals usually offer a much wider bandwidth in free space. Unfortunately, the presence of a ground plane (or a cavity) limits the bandwidth enhancement [3.7]. One way to remedy this limitation is to use absorbers inside the cavity or to terminate the spiral slot with tapered resistive loading [3.8, 3.9], but it reduces the power efficiency. Recently, a bandwidth-enhanced (~15% for AR<3dB) cavity-backed slot antenna has been presented in [3.10], but it requires a complicated feeding network. In this chapter, we develop a broadband cavity-backed loop antenna with a simple feeding structure. The antenna configuration developed is considered to be a combination of a slot loop and a strip loop.

The slot loop has a good CP performance at a lower frequency while the strip loop produces CP radiation at a higher frequency. A combination of the two frequencies leads to a bandwidth enhancement. The slot/strip loop is fed by a single straight microstrip line and a good impedance matching is achieved. The antenna configuration is described in Section 3.1. The operating principle for broadband circular polarization and impedance matching is analyzed in Section 3.2. Finally, experimental results are presented to verify the antenna performance.

3.1 Description of the Antenna

The antenna configuration is shown in Figure 3.1. The radiating element consists of a slot loop and a strip loop (so called a slot/strip loop) with a pair of parasitic slot loops inside the strip loop. The slot/strip loop with the parasitic loops is etched on a thin (thickness=10mils), low-dielectric constant (2.2) substrate (RT/duroid 5880) which is backed by a rectangular cavity. The cavity-backed slot/strip loop is fed by a microstrip feeding line that is fabricated on the same substrate with the slot/strip loop and is placed between the substrate and the cavity. The feeding line is divided into three sections: an open stub, a coupling stub, and a 50-ohms microstrip line. A coaxial line is connected to the 50-ohms microstrip line for the purpose of measurement. The broadband circular polarization is achieved by adjusting the aspect ratio (W_s/L_s) of the slot/strip loop and the depth (D_c) of the cavity. By changing the length (l_{op}) of the open stub and the width (w_{co}) of the coupling stub, a good impedance matching can be obtained. The cavity-backed slot/strip loop antenna was designed for a C-band operation using *Micro-Stripes 7.0*—a transmission-line matrix (TLM) based full-wave electromagnetic simulator [3.11]. The physical dimensions of the antenna are attached in the caption of Figure 3.1.

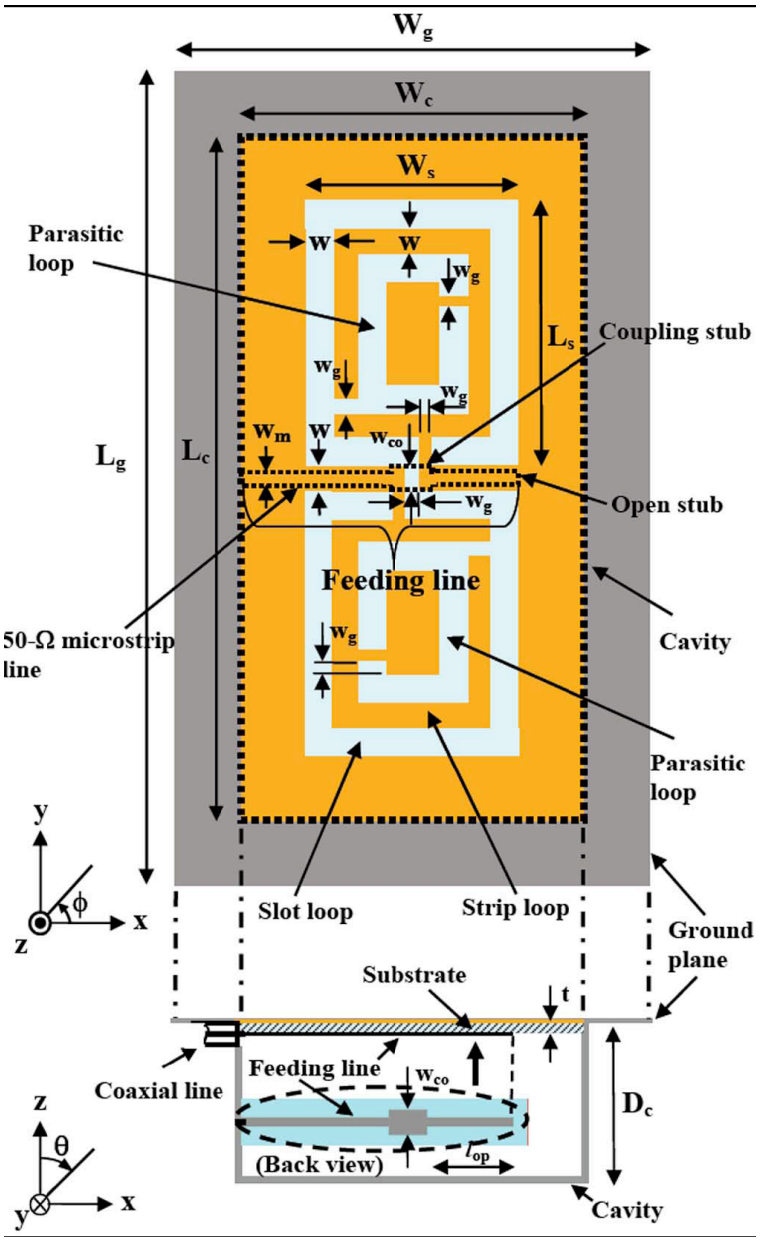

Figure 3.1. Configuration of the cavity-backed broadband CP slot/strip loop antenna. (W_g = 36mm, L_g = 62mm, W_c = 26mm, L_c = 52mm,W_s = 16mm, L_s = 20mm, w = 2mm, w_g = 1mm, w_m = 0:78 mm, D_c = 12mm, t = 0:254 mm; the width (w_{co}) of the coupling stub is w_{co} = w = 2mm, the length of the coupling stub is 3w = 3mm, the length of the open stub is l_{oc} = 6:5 mm.).

3.2 Operating principles of Broadband Circular Polarization

As mentioned in previous sections, the slot/strip loop can be considered as a combination of a slot loop and a strip loop. For the slot loop [Figure 3.2(a)], a pair of shorting strips must be introduced in order to produce a CP wave [3.3], [3.5]. The winding sense of the slot loop decides the sense of its CP radiation, which is left-handed in spatial phase starting from the feeding point (the CP wave is propagating in the z-direction). When a voltage source is enforced at the feeding point, a traveling-wave magnetic current **M** can be excited on the slot loop [3.5]. If the slot loop has a perimeter of approximately one wavelength, the traveling-wave current **M** can create electromagnetic waves in the far-field zone with ~90 degrees of spatial phase as well as time phase, thus achieving CP waves. Due to the nonuniform traveling-wave current distribution along the slot loop, the CP waves created may be not perfect. And the slot loop usually has a narrow bandwidth for CP radiation since the electrical length of the slot loop is frequency dependent. Figure 3.3 shows the AR in the z-direction simulated for the slot loop. It is seen that the slot loop has a minimum AR of >2.5 dB at a lower frequency of ~5.8GHz and a narrow bandwidth of < 5% for AR<3. In order to improve the AR bandwidth, we introduce a strip loop inside the slot loop [see Figure 3.2(b)]. There is a pair of gaps into the strip loop [see Figure 3.2(b)] for the generation of CP radiation [3.12, 3.13]. The strip loop moves the minimum AR to a higher frequency of ~6.8GHz while maintaining a narrow bandwidth (see Figure 3.3). The introduction of the strip loop improves the AR at the higher frequency, but worsens the AR at the lower frequency. For the AR bandwidth enhancement, we need to combine the slot loop and the strip loop into the same antenna aperture. To do so, we introduced a pair of small slots (also with a shorting strip on them) inside the strip loop [see Figure 3.2(c)]. The introduced slots can be considered as a parasitic element of the slot loop, thus improving the bandwidth of the slot loop [3.14, 3.15].

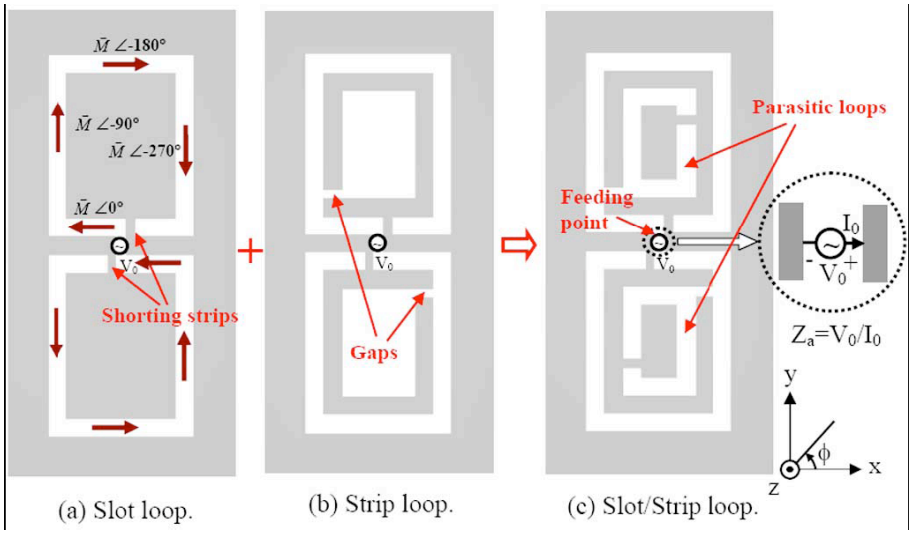

Figure 3.2. Slot/strip loop considered as the combination of a slot loop and a strip loop.

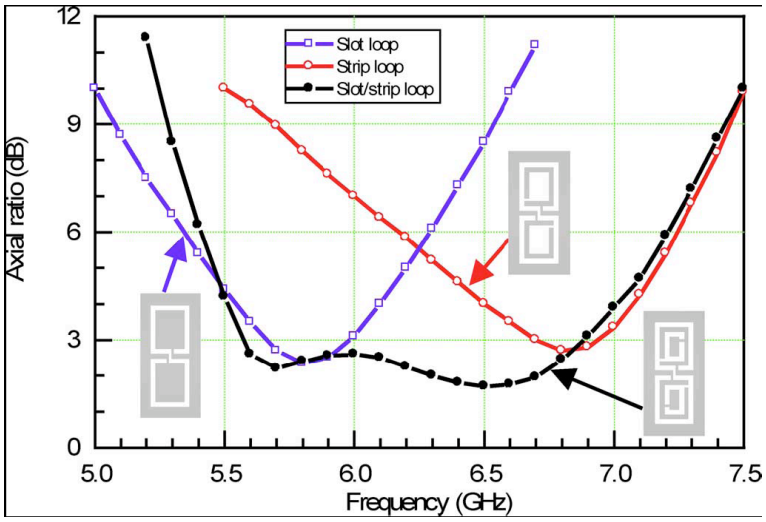

Figure 3.3. Axial ratio for a slot loop, a strip loop, and a slot/strip loop.

Figure 3.3 shows that the AR bandwidth of the slot/strip loop is increased to ~20% for AR<3dB. It should be noted that there would be no bandwidth enhancement without the strip loop (i.e., if the gaps on the strip loop were removed). Therefore, the slot/strip loop cannot be simply thought of as the complementary structure of a wire loop

with parasitic elements [3.15]. The AR bandwidth improvement can be considered as a result of the combination of a strip loop and a slot loop with a pair of parasitic slot loops.

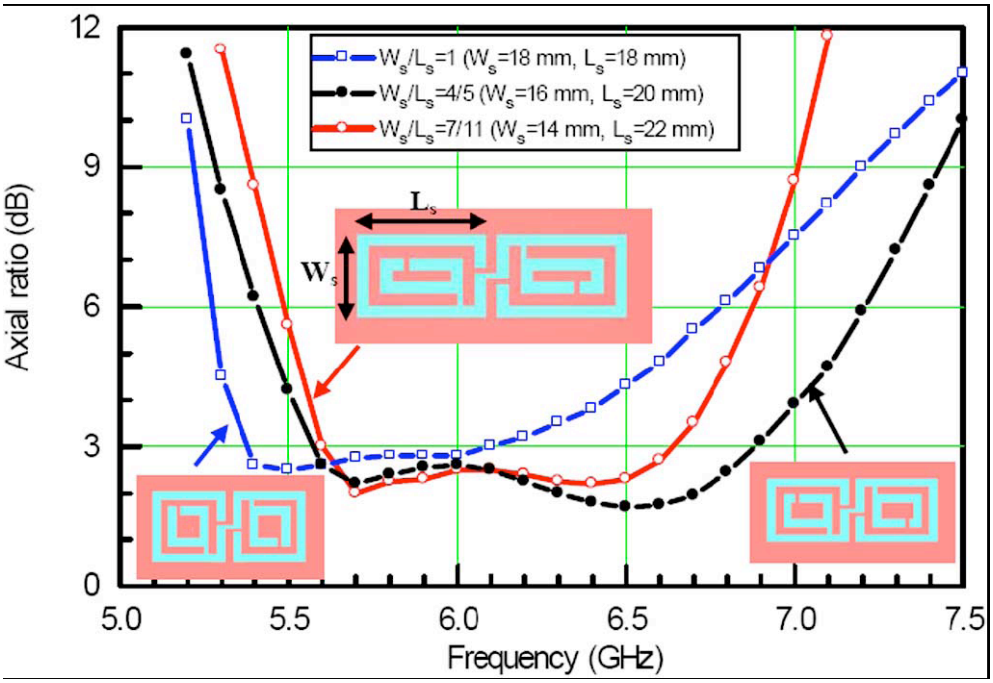

Figure 3.4. Axial ratio at different aspect ratios (W_s/L_s) of the slot/strip loop. (W_c = 28mm and L_c = 48mm for W_s/L_s = 1, W_c = 26mm and L_c = 52mm for W_s/L_s = 4/5, W_c = 24mm and L_c = 56mm for W_s/L_s = 7/11).

The cavity-backed slot/strip loop antenna was optimized by changing the aspect ratio of the loop and the depth of the cavity. Figure 3.4 shows the variation of AR as the aspect ratio (W_s/L_s) is reduced from 1 (i.e., a square) to 7/11. In the optimization, only the width and length of the cavity were adjusted with the aspect ratio to keep the distance (i.e., 5 mm) from the sidewall of the cavity to the edge of the loop unchanged. It is found that the optimized aspect ratio is about 4/5. A larger aspect ratio (e.g., 1) or a smaller aspect ratio (e.g., 7/11) would lead to a narrower AR bandwidth. The variation of AR

with the depth (D_c) of the cavity is displayed in Figure 3.5. At a higher depth (e.g., D_c =14mm), there is a good AR at a lower frequency but a bad AR at a higher frequency. As the depth decreases, the AR is improved at the higher frequency. But if the depth is further reduced (e.g., D_c =10mm), the AR at the lower frequency becomes worse. Therefore there should be an optimal value for the depth, which is found to be D_c=12mm for the proposed slot/strip loop antenna. The effect of the width (W_g) of the ground plane on the AR performance is exhibited in Figure 3.6. There is some insignificant effect due to the diffraction from the edge of the ground plane, that can be resolved by a small readjustment of the slot/strip loop ratio.

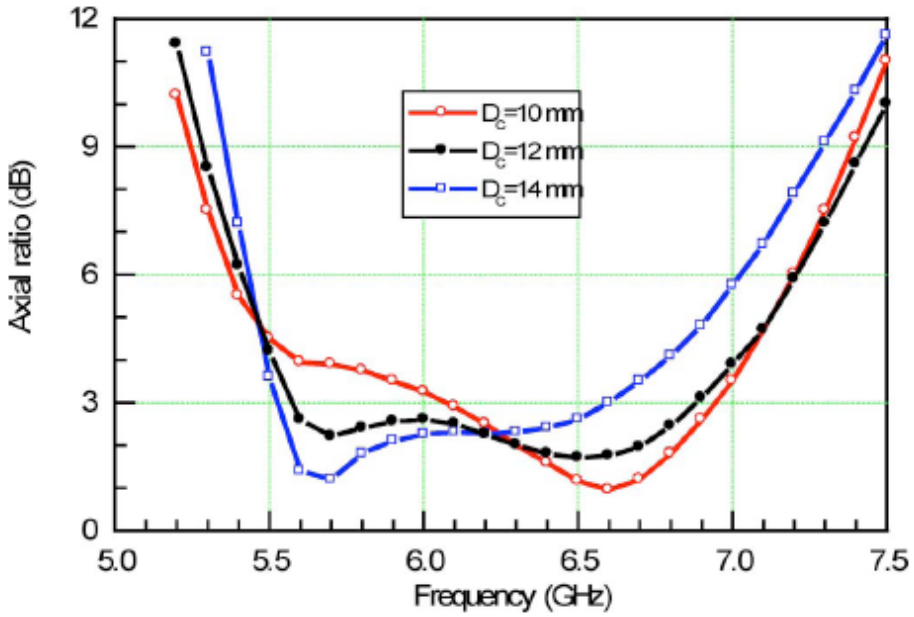

Figure 3.5. Axial ratio at different depths (D_c) of the cavity.

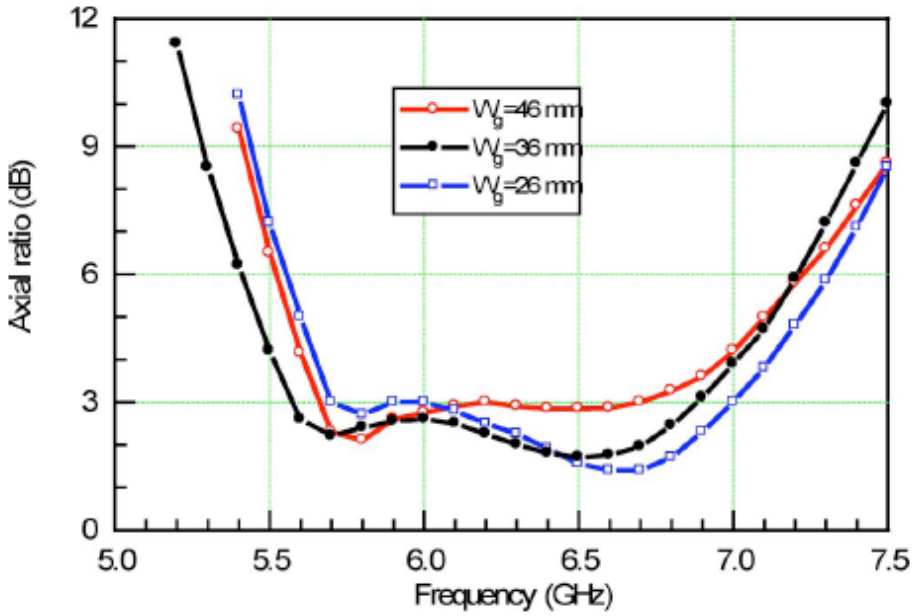

Figure 3.6. The effect of the width (W_g) of ground plane on the axial ratio of the slot/strip loop antenna.

3.3 Experimental results

A prototype of the cavity-backed slot/strip loop antenna is pictured in Figure 3.7. A flexible coaxial cable is connected to the microstrip feeding line for measurement. Figure 3.8 compares the measured return loss (RL) to the simulated result. A slight difference is probably due to the transition between the microstrip line and the coaxial cable. The measured bandwidth for is about 20%. Figure 3.9 shows the comparison of the simulated AR with the measured result. The measured bandwidth for is approximately 22%, but there is a slight bandwidth shift between the AR and RL. The overlapped bandwidth for RL > 10dB is about 19%. The gain of the cavity-backed slot/strip loop antenna is found to be around 9 dBi. The radiation patterns measured at 5.7 GHz and 6.7 GHz are compared with the simulated results in Figure 3.10 and good agreement is

observed for the co-polarization (i.e., the left-hand circular polarization, LHCP) over the main beam. As expected, the beamwidth in the $\phi=0^o$ is wider than that in the $\phi=90^o$ because the length (i.e., W_s) of the antenna aperture in the x-direction is shorter than that (i.e., L_s) in the y-direction. The cross-polarization [i.e., the right-hand circular polarization (RHCP)] is less than -15dB. The discrepancies between the simulated and measured results for the axial ratio, gain, and radiation patterns are mainly due to the measurement errors. We used the *NSI* near-field antenna measurement system. Even though the antenna under test was setup at the far-field zone, the mechanical supporting structures of the system would still cause diffraction, introducing the measurement errors, particularly on the cross-polarized component. But the measurement has indeed demonstrated the broadband CP performance for the proposed antenna.

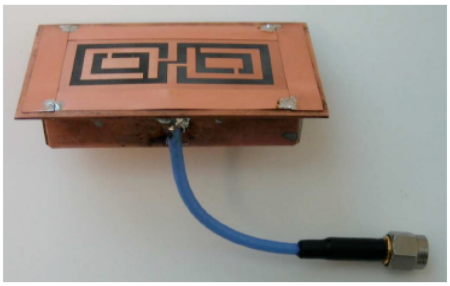

Figure 3.7. Prototype of the cavity-backed slot/strip loop antenna.

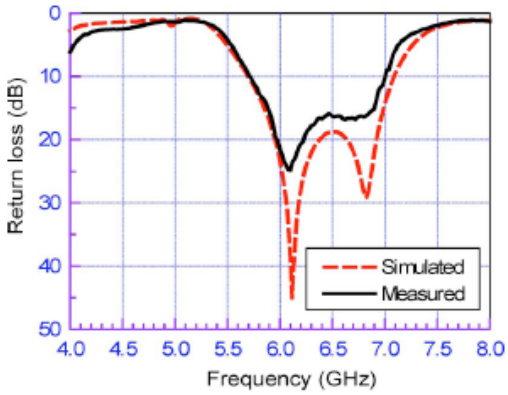

Figure 3.8. Return loss of the cavity-backed slot/strip loop antenna.

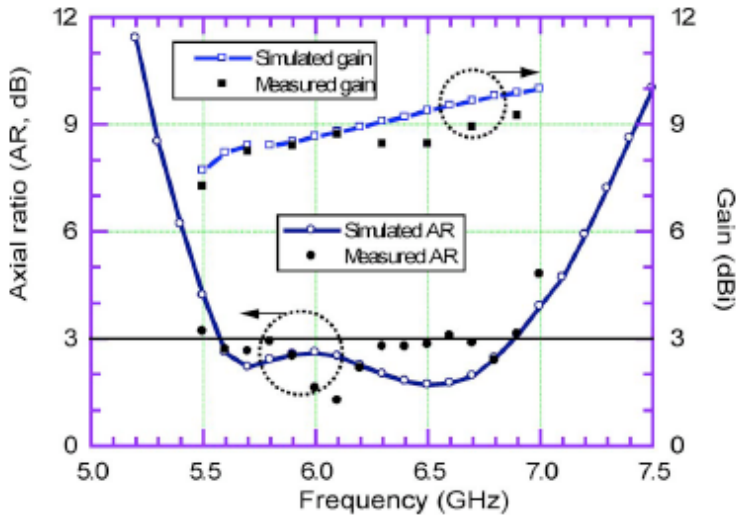

Figure 3.9. Axial Ratio and Gain of the cavity-backed antenna.

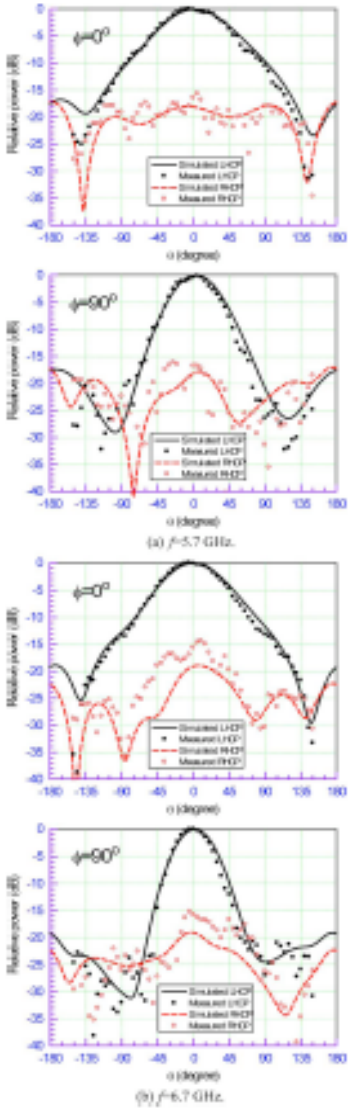

Figure 3.10. Radiation patterns of the cavity-backed slot-strip antenna.

CHAPTER 4

LIQUID ANTENNAS: A NOVEL SOLUTION FOR ENHANCED-RANGE WEARABLE BIOSENSORS AND RFID'S?

One of the major issues for the implementation of Wireless Body Area Networks (WBAN) of these crevices is the very limited range of commonly used metal antennas. Due to the high dielectric constant between the metal antenna material (as well as the metal-based circuitry) and the mostly "ionized-water" human body parts, the near-field gets significantly disturbed, while local reflections due to the dielectric mismatch further shorten the operation range. Even wearable bracelet-like sensing devices have a very low range due to this reason.

Ting and King in 1970 [4.1] proved theoretically that dielectric filled tubes become resonant at specific frequencies. Ida [4.2] demonstrated the dependence of the efficiency bandwidth on the permittivity of the dielectric surrounding a metal conductor. This dielectric slows the velocity of the electromagnetic energy and leads to physically smaller than the purely metallic thin-wire counterparts for the same frequency. An antenna with a salt solution radiator was published by Hatch [4.3], who coined the term "Ionic Liquid Antenna" in 2000, but only indirectly demonstrated its operability in HF frequencies. In this chapter, we propose for the first time the development of liquid antennas, based on aquous salt solutions, operating in microwave frequencies (around 1.7GHz) with significantly improved range and efficiency characteristics, as well as a much simpler and flexible fabrication mechanism. Encapsulating the proposed liquid antennas in flexible plastic containers makes them quite easily wearable or implantable in

the proximity of human organs or biomonitoring devices (e.g. pacemakers) in order to enable short-range wireless communication/control. In addition, corrosion resistance is another advantage of the ionic-liquid, glass/plastic-enclosed antennas, while the easy elimination of air gaps permits shape manipulation and an improved electromagnetic coupling between the probe and the probed dielectric. Since the dielectric property and the conductivity of these solutions are a function of the salinity level as well as of the type of the dissolved salt, these antennas can be easily reconfigured for different areas of mounting/observation.

4.1 Properties of Water Solutions

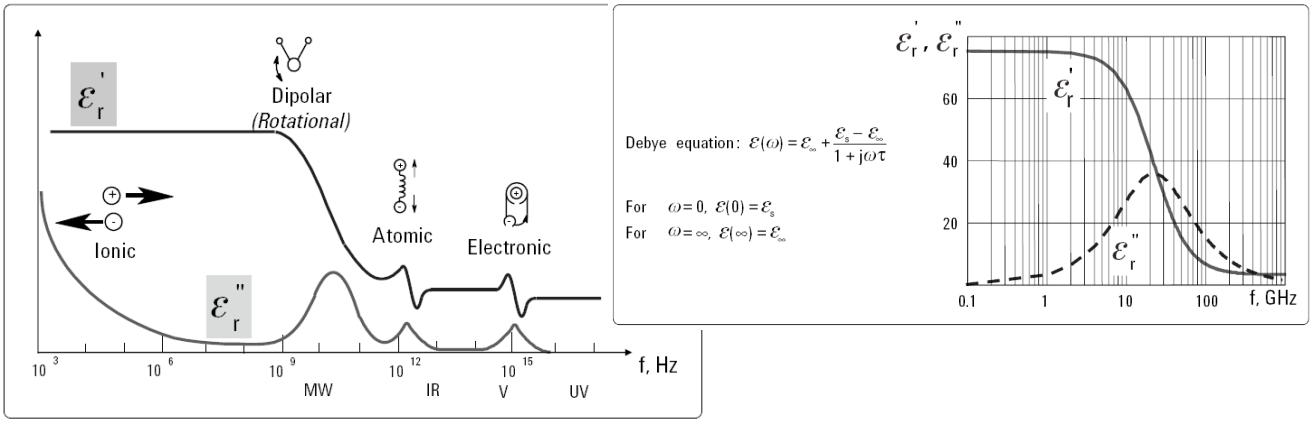

Figure 4.1. Polarization Mechanisms (left), Debye Model (right) [1.26].

The dielectric properties of liquid solutions are shown above in Figure 4.1**.** Although salt-water solutions have demonstrated a significant bandwidth in radiation around 30 MHz, no previous research has been reported in the frequency range of RF and microwave frequencies. The major issue has been the lack of accurate formulas for the dielectric properties of aqueous solutions as a function of frequency, salt type and salinity for these frequencies.

Table 4.1

Common BioTissue Properties from 1.5-2.0GHz

Metal	$\varepsilon_r=1$
Blood	$\varepsilon_r=58$
Skin	$\varepsilon_r=37.5$
Ocean Water	$\varepsilon_r=80$

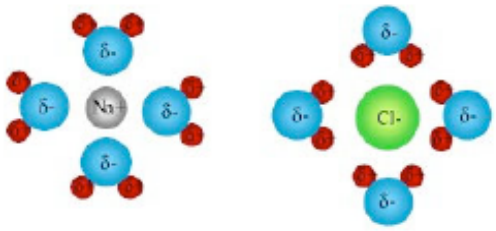

Figure 4.2. Ions in aqueous solutions.

In our simulations, we utilized various dispersive models for the conductivity of the ionized solutions that was observed to change only slightly with frequency in the frequency range of our interest, but very significantly with concentration. Since the addition of salt (NaCl , KCl) lowers the dielectric constant, we utilized the Double-Debye/Cole-Cole for the variation of the dielectric constant ε as a function of frequency ω and concentration c. [4.5]

4.2 Benchmarking Structure Simulations

To verify the performance of the above mentioned liquid antennas, we performed extensive simulations for the structure shown in Figure 4.3. The bracelet-type liquid antenna was made of NaCl aquatic solution (salinity=2.853 mol/Liter, dielectric constant 38 and conductivity 12.4 S/m) inside a very thin plastic container with inner radius of 2.5 mm and was excited with a slot excitation (two electrodes on both sides of the slot). It was mounted on different positions on a multilayer cylinder emulating the human body. This cylinder with the length of 250mm (similar to the lower arm) was composed by two materials: for the inner cylinder with radius r=24mm, the material was blood with dielectric constant 58 and conductivity 1.2 S/m, while for the outer cylindrical ring the material was skin with dielectric constant 37.5 and conductivity 0.6 S/m. The simulation was performed at the central frequency of 1.7 GHz.

Numerous TLM (time-domain) simulations were performed for this structure and the comparative results between a metal (copper) antenna of the same physical size mounted at the same position (30mm from the edge) with liquid antenna are shown in Figures 4.4 (a),(b).

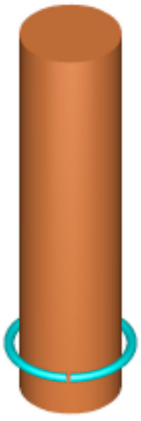

Figure 4.3. Wearable liquid antenna bracelet around the lower-arm phantom.

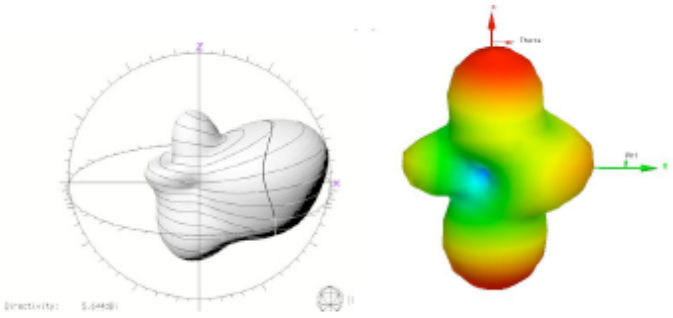

Figure 4.4. Radiation patterns for wearable bracelet: (a-Left) Liquid antenna, (b-Right) Copper antenna around arm phantom.

It can be clearly seen that the liquid antenna has a maximum to the direction transverse to the arm with efficiency of 59% and a directivity of 5.64dBi. On the opposite, the metal antenna has the maximum of its radiation pattern along the direction of the arm, thus minimizing its communication range away from the body. The simulated directivity was 3.36 dBi and the efficiency was 26%. Comparison of the range to the direction that is transverse to the body, and it is usually the most critical dimension for the communication of bracelet-mounted wearable biosensors demonstrated that the liquid antenna led to an improvement by a factor of 12.

Changing the position of the bracelet on the lower-arm phantom, can easily tilt the radiation pattern further improving the directivity and the range of reach. As the bracelet is close to the edge of the arm, the radiation pattern slightly tilts vertically, but still maintains the main pattern characteristics, having the maximum to the direction of the slot. as shown in Figures 4.5 (a),(b). The directivity is 5.86 dBi and 6.44 dBi and the efficiency 61% and 63% respectively for the position of the liquid antenna at 60mm from the bottom edge and at 125 mm from the bottom edge (middle of the arm).

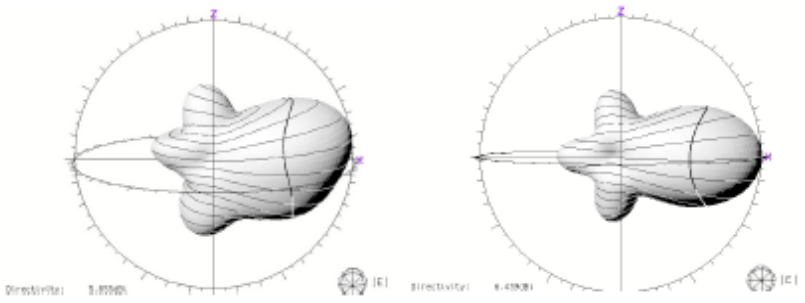

Figure 4.5. Radiation patterns for wearable bracelet liquid antenna: (a) 60 mm from bottom, (b) middle (125 mm from bottom).

One of the most important features of the proposed novel antenna is its very easy reconfigurability by simply changing the salinity levels (or modifying the diluted salt). Time-domain simulations for two different values of salinity (2.853 mol/liter and 4.643 mol/Liter), shown in Figures 4.6 (a),(b) demonstrate that as the salinity increases the pattern gets more isotropic, but maintains the radiation characteristics with a peak to the direction that's transverse to the arm. For Figure 4.6(a) the dielectric constant was 38 with a conductivity value of 12.4 S/m leading to a directivity of 5.64 dBi, while for Figure 4.6(b) the dielectric constant was 23 with a conductivity of 21 S/m. It is clear that the dielectric constant and the conductivity values of the saltwater can be very easily modified by changing the salinity. That would allow the easy reconfigurability of this type of structures in order for them to readjust for different types of tissues, such as internal organs, skin and blood. In addition, that feature would enable the easy re-adjustment and operability of this device in different ambient conditions (desert, polar, space environments) when utilized in wearable applications.

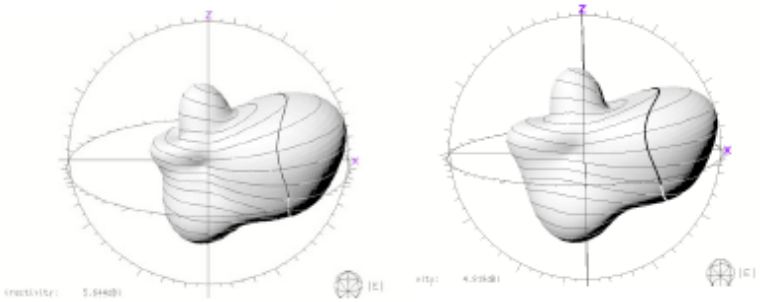

Figure 4.6. Radiation patterns for liquid antenna salinities: (a) 2.853 mol/Liter, (b) 4.634 mol/Liter.

4.3 Experimental Verification

As a proof of concept we realized a real-size prototype of a liquid-dipole operating at 1.7 GHz filled with NaCl in a plastic container that we characterized at Satimo anechoic chamber, using two thin electrodes as the excitation mechanism. As shown in Figure 4.7, very good agreement can be observed between simulations and experiments, something that verifies our assumption that liquid antennas can be easily implemented with a very satisfactory performance in the proximity of the human body.

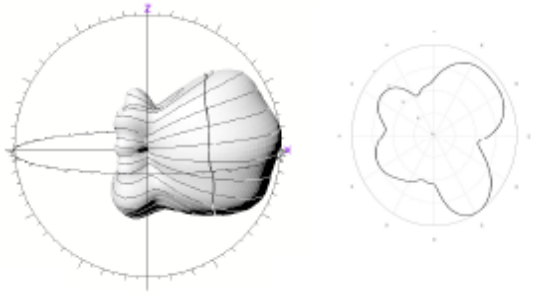

Figure 4.7. Radiation patterns: Simulation (left) and experiments (right).

4.4 Conclusions

We have demonstrated for the first time in RF frequencies the capabilities of the novel concept of liquid antennas for wearable or implantable bio-monitoring applications. Although conventional metal antennas suffer from low range and oxidation problems when in proximity to the human body, the proposed topology features an improved range by an order of magnitude. In addition, it is very conformal allowing for an easy wearable WBAN implementation, as well as it can be very easily reconfigured by adjusting the salinity of the salt solutions in order for it to operate in different ambient conditions. The proposed work could set the foundation for the implementation of truly wireless biosensor networks with small size, lightweight conformal nodes for wireless health monitoring in pharmaceuticals, hospital, ambulance and home-based patient care, as well as in space/underwater missions.

REFERENCES

[1.1] K.Finkenzeller, “RFID Handbook”, 2nd Ed., Wiley, 2004.

[1.2] L.Yang, A.Rida, R.Vyas and M.M.Tentzeris, “RFID Tag and RF Structures on Paper Substrates using Inkjet-Printin g Technology" , IEEE Transactions on Microwave Theory and Techniques, Vol. 55, No.12, Part 2, pp.2894-2901, December 2007.

[1.3] www.impinj.com/files/Impinj_ILT_RFID_World.pdf , Retrieved Feb 2008

[1.4] OD Creutzfeldt, S Watanabe and HD Lux, “Relations between EEG phenomena and potentials of single cortical cells. I. Evoked responses after thalamic and epicortical stimulation”, *Electroencephalogr Clin Neurophysiol., Vol.* 20, pp. 1-18, 1966.

[1.5] J.E. Zimmerman, P. Theine, and J.T. Harding, “Design and operation of stable RF-biased superconducting point-contact quantum devices, etc.”, *Journal of Applied Physics,* Vol. 41, pp.1572-1580, 1970.

[1.6] W.Reich, “Experimentelle Ergebnisse ueber die electrische Funktion von Sexualitat und Angst“ (Sexpolverlag, Copenhagen, 1937). Translated as “Experimental investigation of the electrical function of sexuality and anxiety” in *J. of Orgonomy*, Vol. 3, No. 1-2, 1969.

[1.7] E. Braunwald (Editor), “Heart Disease: A Textbook of Cardiovascular Medicine”, Fifth Edition, p. 108, Philadelphia, W.B. Saunders Co., 1997. ISBN 0-7216-5666-8.

[1.8] M. B. I. Reaz, M. S. Hussain, F. Mohd-Yasin, “Techniques of EMG Signal Analysis: Detection, Processing, Classification and Applications”, *Biological Procedures Online*, vol. 8, issue 1, pp. 11–35, March 2006.

[1.9] F. G. Meyer, G. McCarthy, “Estimation of Baseline Drifts in fMRI”, Information Processing in Medical Imaging. 17th International Conference, IPMI 2001. *Proceedings (Lecture Notes in Computer Science* Vol.2082), p 232-238, 2001.

[1.10] www.mdconsult.com, Retrieved Feb 2008

[1.11] C. L. Baldwin, Auditory Research Group, [archlab.gmu.edu]

[1.12] baseballprospects.com, Retrieved May 2008

[1.13] www.zebris.de Retrieved Jan 2009

[1.14] H. Fayad, P. Record, "Broadband liquid antenna", *Electronics Letters*, Vol. 42, No 3. doi: 10.1049/el:20063633, Feb 2, 2006.

[1.15] Y. Kosta, K. Kosta, "Liquid Antenna Systems", *Proceedings of IEEE APS 2004,* Vol. 3, pp. 2392-2395, June 2004.

[1.16] S. G. O'Keefe, S. P. Kingsley, "Tunability of Liquid Dielectric Resonator Antennas", *IEEE Antennas and Wireless Propagation Letters*, Vol. 6, pp. 533-536, 2007.

[1.17] A. Christ, T. Samaras, A. Klingenböck, N. Kuster, "Characterization of the electromagnetic near-field absorption in layered biological tissue in the frequency range from 30 MHz to 6000 MHz", *Physics in Medicine and Biology,* Vol. 51, pp. 4951-4965, 2006.

[1.18] S. Gabriel, R. W. Lou, C. Gabriel, "The dielectric properties of biological tissues: I. Measurements in the frequency range 10 Hz to 20 GHz", *Phys. Med. Biol*., Vol.41, pp. 2269-2209, 1996.

[1.19] C. Gabriel, S. Gabriel, E. Corthout, "The dielectric properties of biological tissues: II. Literature Survey", *Phys. Med. Biol*., Vol.41, pp 2231-2249, 1996.

[1.20] S. Gabriel, R W Lau, C. Gabriel, "The dielectric properties of biological tissues: III. Parametric models for the dielectric spectrum of tissues", *Phys. Med. Biol.,* Vol. 41, pp. 2271-2293, 1996.

[1.21] A. Christ, T. Samaras, E. Neufeld, A. Klingenböck, N. Kuster, "SAR Distribution in Human Brings When Using Body-Worn RF Transmitters", *Radiation Protection Dosimetry*, Vol. 124, No. 1. pp. 6-14, July 2007.

[1.22] A. Drossos, V. Santomaa, N. Kuster, "The Dependence of Electromagnetic Energy Absorption Upon Human Head Tissue Composition in the Frequency Range of 300-3000 MHz", *IEEE Transactions on Microwave Theory and Techniques,* Vol. 48 No. 11, pp. 1988-1995, November 2000.

[1.23] C. Gabriel, S. Gabriel, E. H. Grant, B. S.J. Halstead, D. Michael P Mingos, "Dielectric parameters relevant to microwave dielectric heating", *Chemical Society Reviews,* Vol. 27, pp. 213-223, 1998.

[1.24] D. Andreuccetti, R. Fossi, C. Petruczi, "An Internet Resource for the calculation of the Dielectric Properties of Body Tissues n the frequency range 10 Hz-100GHz", *IFAC-CNR Institute for Applied Physics*, 1997-2007.

[1.25] "Agilent 85070E Dielectric Probe Kit 200 MHz to 50 GHz: Technical Overview", Agilent Technologies.

[1.26] "Agilent Basics of Measuring the Dielectric Properties of Materials: Application Note", Agilent Technologies.

[1.27] J. B. Jarvis, M. D. Janezic, B. F. Riddle, R. T. Johnk, P. Kabos, C. L. Holloway, R. G. Geyer, C. A. Grosvenor, "Measuring the Permittivity and Permeability of Lossy Materials: Solids, Liquids, Metals, Building Materials, and Negative-Index Materials", NIST (National Institute of Standards and Technology) *Technical Note 1536*, Dec. 2004.

[1.28] label on the back of "Phyto" container.

[2.1] V. Subramanian, P.C Chang, J.B. Lee, S.E Molesa, S.K. Volkman, "Printed organic transistors for ultra-low-cost RFID applications," IEEE Trans. *Components and Packaging Technologies,* Vol.28, No.4, pp.742-747, Dec.2005.

[2.2] Department of Commerce, "Radio Frequency Identification. Opportunities and Challenges in Implementation,", official report, April 2005, http://www.technology.gov/reports/2005/RFID_April.pdf

[2.3] S. Basat, S. Bhattacharya, A. Johnston, S. L. Yang, M. Tentzeris, J. Laskar, "Fabrication and Assembly of a Novel High-Efficiency UHF RFID Tag on Flexible LCP Substrate," Procs. 2006 IEEE *Electronic Components and Technology Conference,*, pp 1352-1355, May 2006, San Diego, CA.

[2.4] J. R. Sanford, "Antenna Design Considerations for RFID Applications," *Crushcraft Corporation,* http://www.cushcraft.com/ Retrieved Feb 2007

[2.5] Crushcraft Corporation, *Antennas for Broadband Wireless, Communications & Data Connectivity*, http://www.cushcraft.com/ Retrieved Feb 2007

[2.6] Poynting Antennas, http://www.poynting.co.za/ Retrieved Feb 2007

[2.7] H. Morishita, K. Hirasawa, and T. Nagao, "Circularly polarized wire antenna with a dual rhombic loop," *IEE Proc.-Microw. Antennas Propag*., vol. 145, no. 3, pp. 219-224, June 1998.

[2.8] R.L Li, N. A Bushyager, J. Laskar, M. M. Tentzeris, "Determination of Reactance Loading for Circularly Polarized Circular Loop Antennas With a Uniform Traveling-Wave Current Distribution," *IEEE Transactions on Antennas and Propagation,* vol. 53, no 12, pp.3920-3929, December 2005.

[2.9] R.L Li, V.F. Fusco, R. Cahill, "Pattern control using a reactively loaded loop antenna," *Antennas and Propagation, 2001. Eleventh International Conference on," vol. 2, pp 766-769, April 2001.*

[3.1] A. Kumar and H. D. Hristov, *Microwave Cavity Antennas*. Norwood, MA: Artech House, 1989, pp. 101–213.

[3.2] K. Fujimoto and J. R. James, Eds., Mobile Antenna Systems Handbook, 2nd ed., Norwood, MA, Artech House, 2000, pp. 461–631.

[3.3] H. Morishita, K. Hirasawa, and K. Fujimoto, "Analysis of a cavity backed annular slot antenna with one point shorted," *IEEE Trans. Antennas Propag.*, vol. 39, no. 10, pp. 1472–1478, Oct. 1991.

[3.4] H. Hirose and H. Nakano, "Dual-spiral slot antennas," *Proc. Inst. Elect. Eng. Microw. Antennas Propag.*, vol. 134, no. 1, pp. 32–36, Jun. 1991.

[3.5] S. Shi, K. Hirasawa, and Z. C. Chen, "Circularly polarized rectangularly bent slot antennas backed by a rectangular cavity," *IEEE Transactions on. Antennas and Propagation*, vol. 49, no. 11, pp. 1517–1524, Nov. 2001.

[3.6] T. Watanabe, K. Hirasawa, and S. Nemoto, "A rectangular-cavity backed cloverleaf slot antenna for circular polarization," in *Proc. 9th Int. Conf. Communications Systems*, Sep. 2004, pp. 595–597.

[3.7] H. Nakano, K. Nogami, S. Arai, H. Mimaki, and J. Yamauchi, "A spiral antenna backed by a conducting plane reflector," *IEEE Tranactions on. Antennas* and *Propagation*, vol. 34, no. 6, pp. 791–796, 1986.

[3.8] T. Ozdemir, J. L. Volakis, and M. W. Nurnberger, "Analysis of thin multioctave cavity-backed slot spiral antennas," *Proc. Inst. Elect. Eng. Microw. Antennas Propag.*, vol. 146, no. 6, pp. 447–454, Dec. 1999.

[3.9] J. L. Volakis, M. W. Nurnberger, and D. S. Filipovic, "A broadband cavity slot spiral antenna," *IEEE Antennas Propag. Mag.*, vol. 43, no. 6, pp. 15–26, Dec. 2001.

[3.10] Q. Li and Z. Shen, "An inverted microstrip-fed cavity-backed slot antenna for circular polarization," *IEEE Antennas Wireless Propag. Lett.*, vol. 1, pp. 190–192, 2002.

[3.11] Micro-Stripes 7.0 Flomerics Group PLC, 2005.

[3.12] H. Morishita, K. Hirasawa, and T. Nagao, "Circularly polarized wire antenna with a dual rhombic loop," *Proc. Inst. Elect. Eng. Microw. Antennas Propag.*, vol. 145, no. 3, pp. 219–224, Jun. 1998.

[3.13] R. L. Li and V. Fusco, "Printed figure-of-eight wire antenna for circular polarization," *IEEE Transactions on Antennas and Propagation*, vol. 50, pp. 1487–1490, Oct. 2002.

[3.14] R. L. Li, G. GeJean, J. Laskar, and M. M. Tentzeris, "Investigation of circularly polarized loop antennas with a parasitic element for bandwidth enhancement," *IEEE Transactions on Antennas and Propagation*, vol. 53, no. 12, pp. 3930–3939, Dec. 2005.

[3.15] R. L. Li, S. Basat, J. Laskar, and M. M. Tentzeris, "Development of wideband circularly polarized square- and rectangular-loop antennas with," *Proc. Inst. Elect. Eng. Microw. Antennas Propag.*, vol. 153, no.3, pp. 293–300, Jun. 2006.

[4.1] C.-Y.Ting and R.King, “The dielectric-filled tubular monopole”, *IEEE Transactions on Antennas and Propagation*, Vol.18, No.5, September 1970, pp.604-610.

[4.2] I.Ida, J.Sato, T.Sekizawa, H.Yoshimura, K.Ito, “Dependence of the efficiency-bandwidth product on electrical volume of small dielectric loaded antennas”, *IEEE Transactions on Antennas and Propagation*, vol. 50, no. 6, June 2002; pp. 821-826.

[4.3] “Dielectric properties of body tissues”, http://niremf.ifac.cnr.it/tissprop/ Retrieved Jan 2006

[4.4] P.Debye, “Polar Molecules”, Dover 1929.

[4.5] R.Somaraju and J.Trumpf, “Frequency, Temperature and Salinity Variation of the Permittivity of Seawater”, *IEEE Transactions on Antennas and Propagation,* vol.54, no.11, November 2006, pp.3441-3448.